

Flexible Fault-Tolerant Topology for Switched Reluctance Motor Drives

Yihua Hu, *Senior Member IEEE*, Chun Gan, *Student Member, IEEE*,
Wenping Cao, *Senior Member, IEEE*, Jiangfeng Zhang, Wuhua Li, *Member IEEE*, Stephen Finney

Abstract—Switched reluctance motor (SRM) drives are one competitive technology for traction motor drives. This paper proposes a novel and flexible SRM fault-tolerant topology with fault diagnosis, fault tolerance and advanced control functions. The converter is composed of a single-phase bridge and a relay network, based on the traditional asymmetrical half bridge driving topology. When the SRM driving system is subjected to fault conditions including open-circuit and short circuit faults, the proposed converter starts its fault diagnosis procedure to locate the fault. Based on the relay network, the faulty part can be bypassed by the single-phase bridge arm while the single-phase bridge arm and the healthy part of the converter can form a fault-tolerant topology to sustain the driving operation. A fault-tolerant control strategy is developed to decrease the influence of the fault. Furthermore, the proposed fault tolerance strategy can be applied to three-phase 12/8 SRM and four-phase 8/6 SRM. Simulation results in Matlab/Simulink and experiments on a three-phase 12/8 SRM and a four-phase 8/6 SRM validate the effectiveness of the proposed strategy, which may have significant economic implications in traction drive systems.

Index Terms—Fault diagnosis, fault tolerance, traction motor drive, switched reluctance motor (SRM).

K_L'	Inductance slope when faulted
K_i	Current slope when faulted
L_{\min}	Minimum of the phase inductance
L_{\max}	Maximum of the phase inductance
T^*	Given load torque
T	Instantaneous torque
T_{av}	Average electromagnetic torque of one phase when normal
T_{av}'	Average electromagnetic torque of one phase when faulted
U_{in}	Bus voltage
ω_r	Angular velocity
θ_{on}	Turn-on angle
θ_{off}	Turn-off angle
R_{eq}	Equivalent resistance of loop
θ_p	Phase current ending angle
$i_s(\theta)$	Instantaneous phase current

NOMENCLATURE

D	PWM duty-cycle
i_a, i_b, i_c	Currents for phases A, B and C
i_{\max}'	Phase current peak when faulted
i_{\max}	Phase current peak when normal
Δi	Hysteresis window
N_r	Rotor poles
K_L	Inductance slope when normal
K_i'	Current slope when normal

Manuscript received June 3, 2015; revised August 8, 2015 and August 23, 2015; accepted August 24, 2015. This work is sponsored by the EPSRC of UK (EP/L00089X/1) and NSFC of China (51361130150).

Copyright © 2010 IEEE. Personal use of this material is permitted. However, permission to use this material for any other purposes must be obtained from the IEEE by sending a request to pubs-permissions@ieee.org.

Y. Hu is with the College of Electrical Engineering, Zhejiang University, Hangzhou, 310027, China; and the Department of Electronic and Electrical Engineering, University of Strathclyde, Glasgow, U.K.

C. Gan and W. Li are with the College of Electrical Engineering, Zhejiang University, Hangzhou 310027, China (e-mail: ganchun.cumt@163.com).

W. Cao is with the School of Electronics, Electrical Engineering and Computer Science, Queen's University Belfast, Belfast, U.K.

J. Zhang and S. Finney are with the Department of Electronic and Electrical Engineering, University of Strathclyde, Glasgow, UK.

I. INTRODUCTION

Over the recent decades, the development of electric vehicles (EVs) and hybrid electric vehicles (HEVs) is considered to be a key measure to reducing CO₂ emission and environmental pollution [1]-[5]. Switched reluctance motors (SRMs) are characterized with rare-earth-free and wide-speed-range advantages, and are becoming an attractive technology for EV/HEV applications [6]-[12]. Due to the harsh operational environments and repetitive duty cycles, power electronic devices in traction drives are prone to failure in the transient of speed up and braking [13]-[14]. Therefore, high reliability and fault tolerance are of critical importance in EV/HEV applications.

In SRM drives, the asymmetrical half-bridge topology is the most widely used converter topology. Its fault diagnosis (such as short circuit and open circuit) is researched in papers [15]-[21]. For example, paper [16] uses the bus current, paper [17] uses the freewheeling current and paper [18] uses the phase current to distinguish open-circuit from short-circuit faults. Other analytical methods, such as fast Fourier transformation (FFT), genetic algorithm based artificial neural network and fuzzy logic are introduced in fault diagnosis [19]-[21]. The SRM fault is also studied in [22]-[24]. By

injecting high-frequency pulses, the faulty phase winding can be identified and the fault category also can be determined [24].

For the fault tolerance SRM structure, increasing the number of phase in SRMs is a common method [25]-[26]. Dual channels are also developed to improve the reliability of SRM driving systems [27]. A modular stator structure is developed to bypass the fault winding [28], [29]. In [30], a double-layer-per-phase isolated SRM is proposed to improve the fault-tolerant capability.

Fault tolerance converter topology for SRM drive systems are studied in papers [31]-[32]. In order to decrease the impact of faults on the drive performance, paper [31] proposes a new topology with two switching devices added to the traditional asymmetric half bridge topology; while it is not in modular structure. A decentralized topology is developed in [32] to make full use of independent phase windings but a large number of power switching devices are needed. A three-phase bridge inverter is adopted in [33] and the corresponding fault

tolerance scheme is also developed. However, the converter cannot bypass the faulted winding.

For fault tolerance control, artificial neural network and genetic algorithm are developed [34]. The fuzzy logic control without a model is proposed in [35] to improve the performance of the SRM under faulty conditions. In the absence of position sensors, a fault tolerance control strategy is proposed in [36] to deal with the phase-absent operation. Traditional asymmetrical half bridge topology can provide fault tolerance if the SRM drive is partially faulted with the absence phase operation. In case faults occur in all phases, the SRM drive will stop working. Paper [37] proposes a fault tolerance topology with a modular structure. There is a single extra connection node per phase. In case a fault occurs, this fault tolerance topology only can save 1/2 winding in the faulted phase. Besides, it also requires three half-bridge legs for fault tolerance operation. A comparison of the fault tolerance methods is illustrated in Table I. It can be seen that the current strategies can provide some fault tolerance functions.

TABLE I COMPARISON OF FAULT TOLERANCE METHODS

Topology Item	Traditional SRM system [18]	Specially designed motor [28][30]	Fault tolerance topology Paper [32] Paper [31]		Expected fault tolerance structure
Motor	Traditional SRM	Special design	Special design	Traditional SRM	Traditional SRM
Converter modular structure	Yes	Yes	Yes	No	Yes
Fault diagnosis	Complicated	N/A	Easy	N/A	Easy
Fault tolerant operation ability	Achievable with phase absence	Achievable with phase absence	Achievable without phase absence	Achievable with phase absence	Achievable without phase absence
Cost	Low	High	High	Medium	Low

In order to satisfy the application requirements, the fault tolerance SRM drive system should requires the following conditions: (i) without change the traditional SRM structure; (ii) easy to fault diagnosis; (iii) adapt to all kinds of converter and phase winding fault; (iv) fault tolerance topology with module structure that suits for massive production; (v) relative low cost; (vi) adapt to both three-phase SRM and four-phase SRM drive system. This paper is set out to develop a highly fault-tolerant SRM drive with the flexible converter topology to match the above conditions. In section II, the proposed fault diagnosis topology and strategy is introduced; in section III, fault tolerance operation control strategy is illustrated; the popularization and application of proposed method is presented in section IV; simulation and experiment are given in section V; the final part is conclusion.

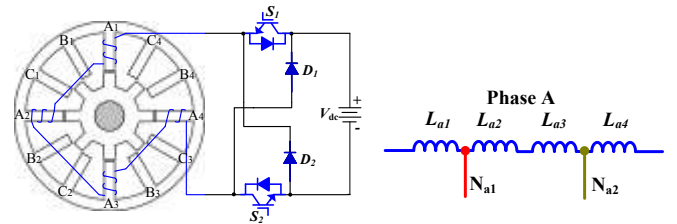
II. FAULT DIAGNOSIS TOPOLOGY AND STRATEGY

A new fault tolerance topology is developed to improve the system performance that also can improve SRM driving system fault tolerance ability.

A. Proposed Fault Tolerance Topology

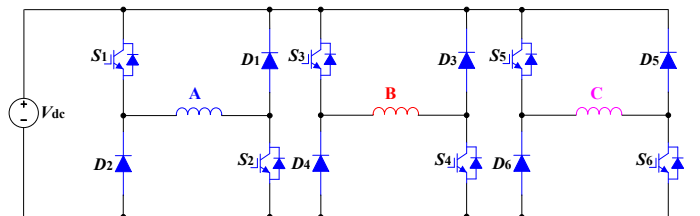
Traditionally, for a three-phase 12-slot/8-pole (12/8) SRM, each phase is composed of four series-connected windings, as shown in Fig. 1(a). For phase A, the connection nodes for four winding are marked as N_{a1} and N_{a2} , as presented in Fig. 1(b).

The asymmetrical half bridge is employed as the driving topology, as shown in Fig. 1(c). In Fig.1 (c), S_1, S_3 and S_5 are upper switching devices, S_2, S_4 and S_6 are lower switching devices; $D_1 \sim D_6$ are freewheeling diodes. In order to locate the fault position precisely, each phase converter is divided into three parts (I-III), as illustrated in Fig. 1(d).

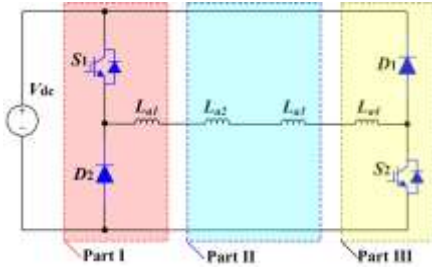


(a) Phase converter of 12/8 SRM

(b) Phase winding tapping node



(c) 12/8 driving topology



(d) Three components of each phase converter.

Fig. 1. Basic winding structure and driving topology of a 12/8 SRM.

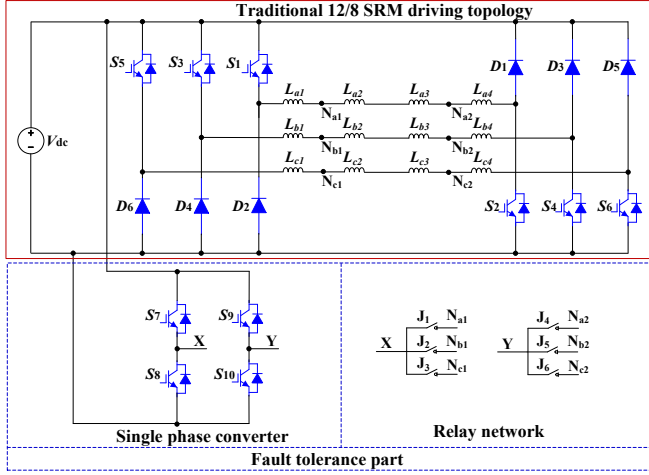


Fig. 2. Fault tolerance topology for a 12/8 SRM.

B. Open-Circuit Faults Diagnosis

Open-circuit faults are common fault phenomena in the SRM driving system. In the traditional asymmetrical half bridge topology, when an open circuit occurs in a phase converter, the corresponding phase is out of operation, and the SRM will work in a phase absence operation. The machine torque becomes unbalanced and the torque ripple is increased. The signature of such a fault is zero current in a phase converter, which is easy to pick for diagnosis purposes. In order to achieve fault tolerance operation, the fault part of phase converter should be located. The flowchart of single-phase open-circuit diagnosis is shown in Fig. 3. First, the diagnosis system checks if the phase current is always 0. If this is the case, the system takes the following actions. J_1 is switched on and S_2 is switched off; then the controller gives driving signal to S_7 , S_7 and S_8 . If the phase A converter can operate, part I is healthy; otherwise, part I is faulty. Next, switched on J_4 and give the signal of S_7 , S_9 and S_{10} , if the phase A still can operate, part II is healthy and part III is unhealthy. Otherwise, part II is unhealthy and part III is healthy. When multi-phase fault occurs; the fault diagnosis is carried out phase by phase, each phase fault diagnosis progress is the same as Fig. 3 with enabling corresponding relays and switching devices.

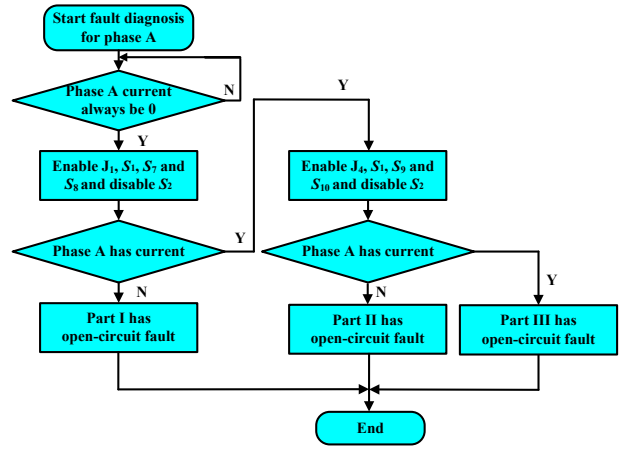


Fig. 3. Flowchart of the open-circuit fault diagnosis.

C. Fault Tolerance Operation under Open-Circuit Fault Conditions

Due to the central symmetry of phase converter, there are two kinds of fault tolerance operation modes. The first one is part I and part III fault scenario. The other one is part II fault scenario.

When part I is under fault condition, by turning on relay J_1 , the fault tolerance bridge arm (composed by S_7 and S_8) and the healthy parts form new topology; the corresponding working states are presented in Fig. 4 (a)~(c). In the newly-formed fault tolerance operation topology, when S_7 and S_2 conduct, the excitation circuit is shown in Fig. 4(a). Fig. 4(b) presents the energy-recycling mode, in which the winding voltage is $-V_{dc}$ to speed up winding demagnetization. Fig. 4(c) shows the freewheeling conduction mode, in which the winding L_{a2} , L_{a3} and L_{a4} voltage is 0. Similarly, when the part III is under fault condition, switch on relay J_4 , the fault tolerance bridge arm (composed by S_9 and S_{10}) the healthy parts form a new topology to sustain operation.

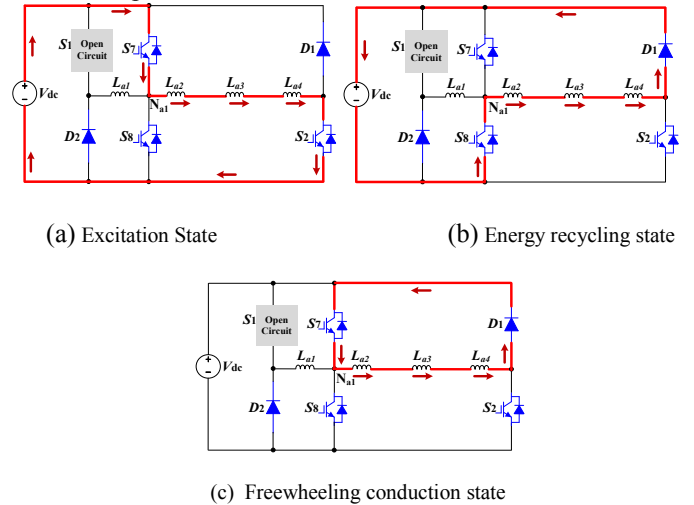


Fig. 4 Working states under part I fault conditions.

When part II is under fault condition, switch on relay J_1 and J_4 , the bridge arm is composed by S_7 and S_8 , and the part I form one topology; the bridge arm is composed by S_9 and S_{10} , and the part III form the other topology. Two topologies work together

to decrease the influence of part II open circuit. The corresponding working states are presented in Fig.5 (a)~(c).

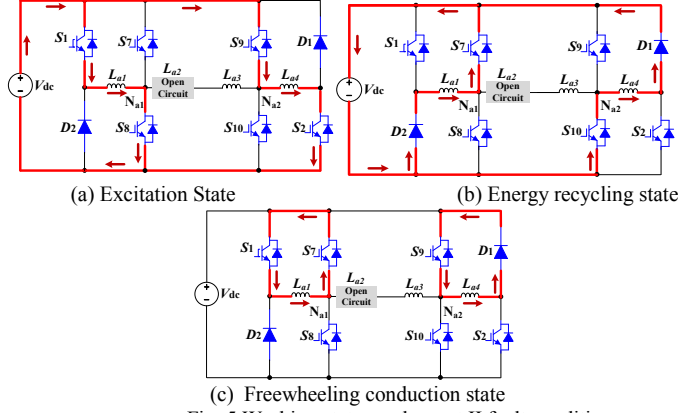


Fig. 5 Working states under part II fault conditions.

When multiple phases have faults at the different parts, as show in Fig. 6; the part I of phase A and the part III of phase B are in open circuit fault condition. Switch on relay J_1 , bridge arm composed by S_7 and S_8 is employed by phase A to form new topology to realized fault tolerance operation of phase A; switch on relay J_5 , bridge arm composed by S_9 and S_{10} is employed by phase B to form new topology to realized fault tolerance operation of phase B. The corresponding working states are presented in Fig.6 (a) ~ (f). Fig.6 (a) ~ (c) are three working states of phase A; Fig.6 (d) ~ (f) are three working states of phase B.

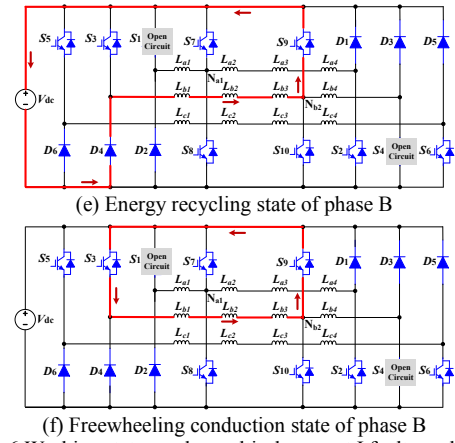
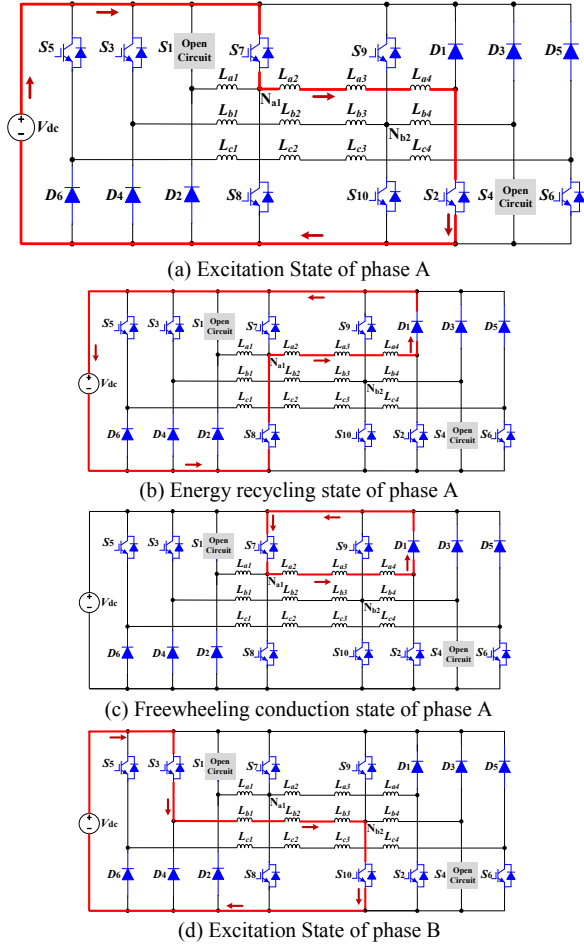


Fig. 6 Working states under multi-phase part I fault condition.

The proposed fault tolerance strategy can also operate in different winding open circuit fault conditions. When L_{a1} , L_{b1} and L_{c1} are open circuited, as shown in Fig.7 (a), by enabling relay J_1 , J_2 and J_3 , bridge arm composed by S_7 and S_8 is employed by phase A, B and C to form new topology to realized fault tolerance operation, in which S_7 is with the function of publish switching devices. The other fault scenario is different part in different phases, as shown in Fig. 7(b), by enabling relay J_1 , J_3 , J_5 and J_6 , the both half bridge arms are employed by phase A, B and C to form new topology to realized fault tolerance operation. For phase A, S_7 , S_8 , D_1 and S_2 form new driving topology; for phase B, S_3 , D_4 , S_9 and S_{10} form new topology; for phase C, S_7 , S_8 , S_9 and S_{10} form new topology.

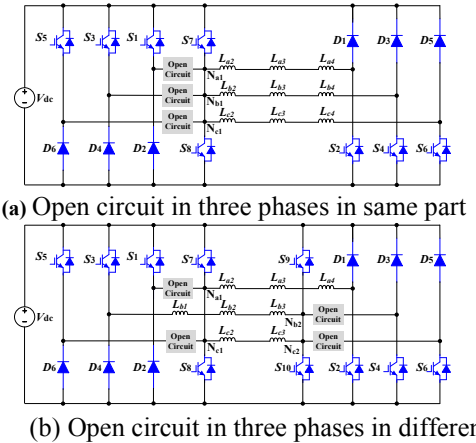
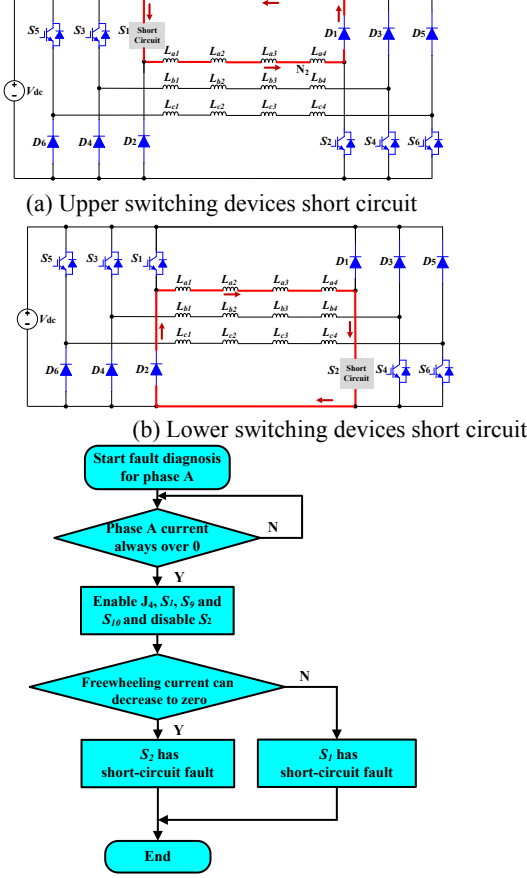


Fig. 7 Open circuit fault scenario in windings.

D. Switching Device Short-Circuit Fault Diagnosis

Switching devices short circuit and inner-turn short circuit are the two causes for short-circuit faults. For the inner-turn short circuit, the phase windings still can operation; nevertheless, when converter is under switching device short-circuit fault condition, the freewheeling current cannot decrease to zero after turning off switching devices of phase converter, which leads to negative torque that influence SRM system operation. When the upper switching device of phase A is short-circuited, the only freewheeling mode is illustrated in Fig. 8(a); the same theory, when the lower switching device of phase A is short-circuited, the only freewheeling mode is illustrated in Fig. 8(b). As illustrated in Fig. 8, because there is no energy recycling loop, the corresponding phase current is

always over zero that can be employed in short-circuit fault diagnosis. Fig. 8(c) shows a flowchart of the diagnosis of switching device short-circuits. When the phase current is always higher than zero, the corresponding phase is short circuited. After enabling J_4 , S_7 , S_9 and S_{10} to form a new converter and if the phase current decreases to zero, S_2 is proven to be short circuited. If the phase current is still over zero, S_7 is short circuited.



(c) Flowchart for the diagnosis of the switching device short-circuits. Fig. 8 Fault diagnosis and tolerance under switching devices short circuit faults.

E. Fault Tolerance Operation under Hybrid Fault Conditions

When SRM traditional asymmetrical half bridge topology is under hybrid fault conditions, in which both open circuit and short circuit occur in the traditional topology, the fault tolerance part can help SRM to achieve fault tolerance operation. Fig. 9(a) presents the scenario of all upper switching devices are under fault condition, in which S_7 and S_3 are under short-circuit fault and S_5 are under open-circuit fault condition; in traditional topology, the traditional topology can not work under Fig. 9(a) fault condition. In the proposed fault tolerance topology, the relay J_1 , J_2 and J_3 are switched on, and the bridge arm composed S_7 and S_8 is activated to form new topology, as shown in Fig.9 (b); In the new topology, the fault part of each phase are blocked; the S_7 is acted as public switching devices, and the three phases all can operate, in which only 1/4 part of phase winding can not output torque. Fig.9 (c) is the hybrid fault scenario 2, in which upper switching device S_7 is under short circuit fault, upper switching device S_5 is under open

circuit, and lower switching device S_7 is under short circuit fault condition. Switch on J_1 , J_3 and activate S_7 and S_8 , faulty S_7 and S_5 can be blocked; switch on J_5 , and activate S_9 and S_{10} , faulty S_4 can be blocked; the fault tolerance state is presented in Fig. 9 (d). Fig.9 (e) shows the hybrid fault scenario 3, in which fault occurs at different phases and different parts. Switch on J_1 , J_3 , J_4 and J_5 , single phase bridge is activated, as presented in Fig.9 (f).

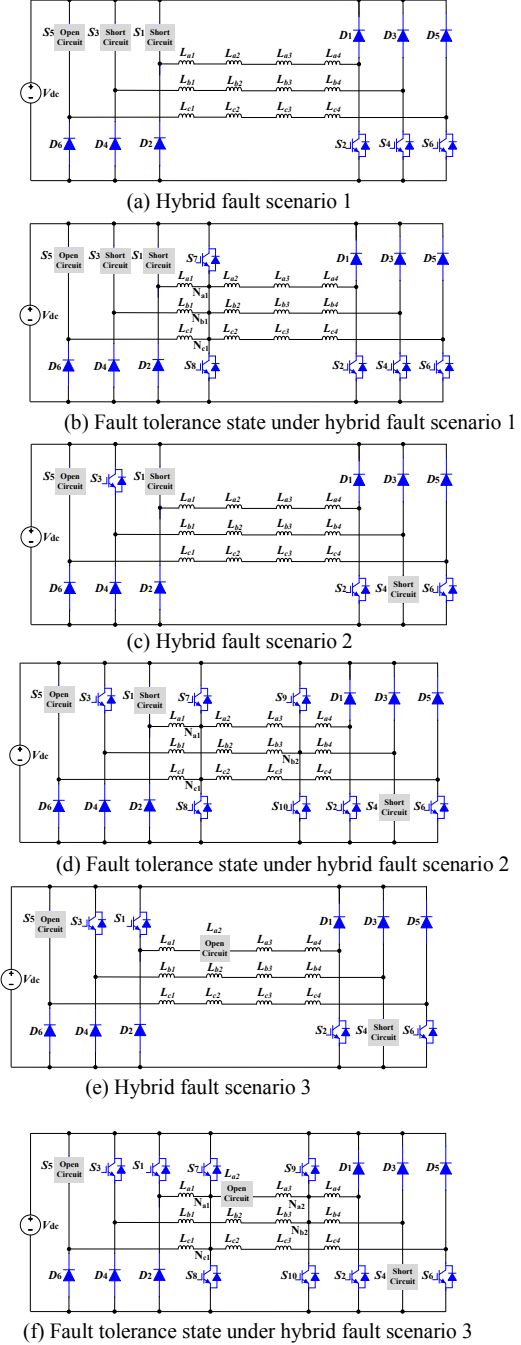


Fig. 9 Hybrid fault scenarios.

F. Fault Tolerance Topology Formation Rule

In order to maintain phase independence, when part II of each phase converter is healthy, two phase nodes all connected with bridge arms is not allowed. When part II of phase converter is faulty, the corresponding faulty phase can connect with both bridge arms without influence of other phase. As shown in Fig.10, although J_1 , J_2 , J_4 and J_5 are switched on, L_{a2} is

open circuit that there is no loop in part windings of phase A (L_{a2} and L_{a3}) and part windings of phase B (L_{b2} and L_{b3}).

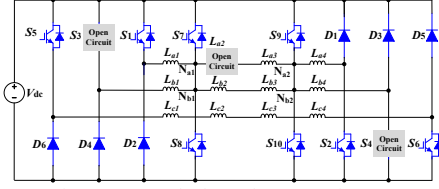


Fig. 10 Part II fault, node connection.

There are only two bridge arms in the fault tolerance part. Due to the traditional topology central symmetry, one bridge arm can block the part I fault of phase converter; the other bridge arm can block the part III fault of phase converter; when the part II of phase converter is in open circuit condition, both bridge arms can support the corresponding faulty phase to achieve fault tolerance operation, as shown in Fig. 5. Therefore, the two bridge arms can support all kind of fault tolerance operation. The extremely fault condition is shown in Fig. 11; the shadow part of converter is broken, and only part II of phase A converter is healthy; by the proposed fault tolerance topology, the SRM still can operate by the converter formed by single phase bridge and phase winding L_{a2} and L_{a3} .

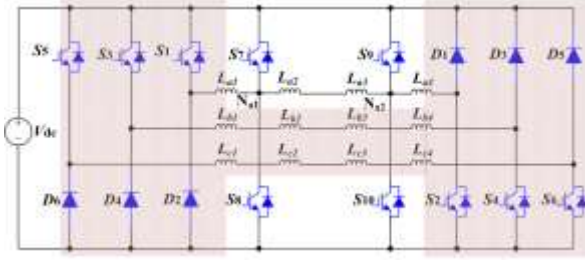


Fig. 11 Extreme fault tolerance operation condition.

III. FAULT TOLERANCE OPERATION CONTROL STRATEGY

Because the fault tolerance topology and phase winding node connection are developed, the corresponding control strategy especially fault tolerance operation is needed to deal with the faulty condition.

G. Control Schemes for SRM Drives under Healthy Condition

When the SRM driving system is in healthy condition, the fault tolerance topology stays in idle mode, and the system is the same as the traditional asymmetrical half bridge topology; the current chopping control (CCC) and voltage-PWM control are employed as two basic schemes. According to the given speed ω^* , the CCC is activated at low speed condition; while voltage-PWM control is activated at high speed condition, as illustrated in Fig. 12. The speed controller (e.g. proportional integral (PI) controller) is used to regulate the motor speed. The motor speed is measured by an encoder. The turn-on and turn-off angles are determined by a commutation controller. The fault protection is provided to deal with switching devices faults and phase winding faults and so forth. In the CCC system, the phase current is addressed by a current controller. The current reference i^* is derived from the speed controller. The instantaneous phase currents are measured by current sensors, and fed back to the threshold logic to calculate i_{max} and i_{min} that determine the switching states in each phase turn-on region. In the voltage-PWM control system, the phase voltage is addressed by a voltage controller. The PWM duty-cycle is

derived from the speed controller, and regulated according to the instantaneous speed. The average voltage applied to the phase winding is chopped down to the value DV_{dc} with a duty-cycle D .

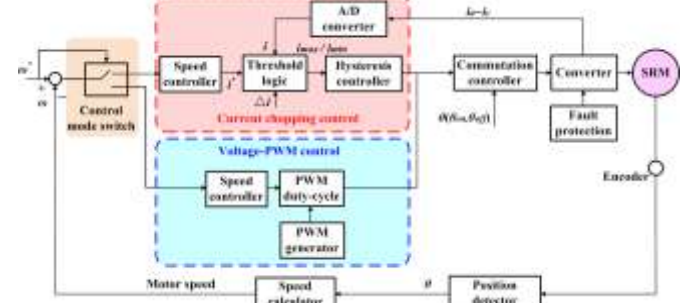


Fig. 12. SRM control strategy under healthy condition.

H. Fault Tolerance Control under Unhealthy Conditions

When part I or part III of the traditional asymmetrical half bridge is under fault condition, the fault tolerance topology can be formed by switching on corresponding fault tolerance part. In this process, the fault part can be blocked, and the healthy part still can work.

Fig. 13 illustrates the relationship between the phase current, phase inductance and rotor position. In the figure, θ_{on} and θ_{off} are the turn-on and turn-off angles, i_1 and L_1 are the phase current and phase inductance in normal conditions, i_2 and L_2 are the phase current and phase inductance in fault tolerance under part I fault conditions, and i_3 and i_4 are the phase currents when the turn-on angle is set lagged. Fig. 13(a) presents the phase current and phase inductance in the fault tolerance operation with 3/4 phase winding. Due to the decrease of phase inductance under fault condition, the phase current has higher current amplitude. Under fault condition, by controlling the turn-on angle, the phase current also can be controlled as in normal condition. The corresponding phase current is shown in Fig. 13 (b). The waveforms are similar to the faulted case in part III.

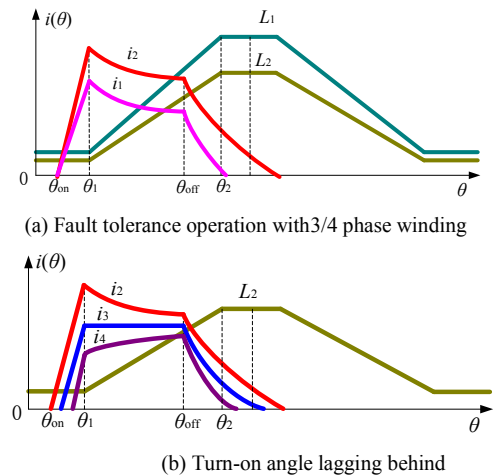


Fig. 13. Relationship between the phase current and phase inductance under part I fault condition.

The phase inductance slope in the inductance-ascending region is given by

$$K_L = \frac{L_{max} - L_{min}}{\theta_2 - \theta_1} \quad (1)$$

where L_{\min} and L_{\max} are the minimum and maximum of the phase inductance, and θ_1 and θ_2 are the relevant rotor positions.

In the region of $\theta_{\text{on}} \leq \theta < \theta_1$, the phase current is expressed as

$$i(\theta) = \frac{\theta - \theta_{\text{on}}}{\omega_r \cdot L_{\min}} V_{dc} \quad (2)$$

where V_{dc} is the bus voltage, and ω_r is the rotor angular velocity. The phase current increases quickly in this region, and the current slope factor K_i satisfies

$$K_i = \frac{di}{d\theta} = \frac{V_{dc}}{\omega_r \cdot L_{\min}} > 0 \quad (3)$$

In the region of $\theta_1 \leq \theta < \theta_{\text{off}}$, the phase current is expressed as

$$i(\theta) = \frac{V_{dc}}{\omega_r} \frac{\theta - \theta_{\text{on}}}{L_{\min} + K_L (\theta - \theta_1)} \quad (4)$$

The peak of the phase current is at θ_1 can be written by

$$i_{\max} = \frac{\theta_1 - \theta_{\text{on}}}{\omega_r \cdot L_{\min}} V_{dc} \quad (5)$$

The average electromagnetic torque of one phase can be expressed as

$$T_{av} = \frac{N_r V_{dc}^2}{2\pi \omega_r^2} (\theta_{\text{off}} - \theta_1) \left(\frac{\theta_1 - \theta_{\text{on}}}{L_{\min}} - \frac{1}{2} \frac{\theta_{\text{off}} - \theta_1}{L_{\max} - L_{\min}} \right) \quad (6)$$

where N_r is the rotor poles.

If the SRM system has an open-circuit or short-circuit fault in part I or part III of the converter, the proposed fault tolerance converter will operate with 3/4 part of the fault phase winding, and the new phase inductance can be expressed as

$$\begin{cases} L_{\max}' = \frac{3}{4} L_{\max} \\ L_{\min}' = \frac{3}{4} L_{\min} \end{cases} \quad (7)$$

where L_{\min}' and L_{\max}' are the minimum and maximum of the phase inductance in fault tolerance operation.

In the inductance ascending region, the phase inductance slope can be expressed as

$$K_L' = \frac{3}{4} \frac{L_{\max}' - L_{\min}'}{\beta_s} = \frac{3}{4} K_L \quad (8)$$

In the region of $\theta_{\text{on}} \leq \theta < \theta_1$, the phase current slope in fault-tolerant operation is given by

$$K_i' = \left(\frac{di}{d\theta} \right)' = \frac{V_{dc}}{\omega_r \frac{3}{4} L_{\min}} = \frac{4V_{dc}}{3\omega_r L_{\min}} = \frac{4}{3} K_i \quad (9)$$

In fault-tolerant operation, at the position $\theta = \theta_1$, the peak of the phase current can be written by

$$i_{\max}' = \frac{V_{dc}}{\omega_r} \frac{\theta_1 - \theta_{\text{on}}}{\frac{3}{4} L_{\min}} = \frac{V_{dc}}{\omega_r} \frac{4(\theta_1 - \theta_{\text{on}})}{3L_{\min}} = \frac{4}{3} i_{\max} \quad (10)$$

The average electromagnetic torque is expressed as

$$T_{av}' = \frac{N_r V_{dc}^2}{2\pi \omega_r^2} (\theta_{\text{off}} - \theta_1) \left(\frac{\theta_1 - \theta_{\text{on}}}{\frac{3}{4} L_{\min}} - \frac{1}{2} \frac{\theta_{\text{off}} - \theta_1}{\frac{3}{4} L_{\max} - \frac{3}{4} L_{\min}} \right) = \frac{4}{3} T_{av} \quad (11)$$

Clearly, the peak of the phase current, and the average electromagnetic torque of the failure phase are 4/3 of the normal value when working in the fault-tolerant operation.

If the voltage drop which is caused by winding resistance and solid state devices is considered, the equation (11) can be revised as:

$$T_{av}'' = \frac{N_r V_{dc}^2 [1 - R_{eq} \sqrt{\frac{N_r}{2\pi}} \int_{\theta_{\text{on}}}^{\theta_p} i_s^2(\theta) d\theta]^2}{2\pi \omega_r^2} (\theta_{\text{off}} - \theta_1) \left(\frac{\theta_1 - \theta_{\text{on}}}{\frac{3}{4} L_{\min}} - \frac{1}{2} \frac{\theta_{\text{off}} - \theta_1}{\frac{3}{4} L_{\max} - \frac{3}{4} L_{\min}} \right) \quad (12)$$

where R_{eq} is the equivalent resistance of loop, θ_p is the phase current ending angle, $i_s(\theta)$ is the instantaneous phase current.

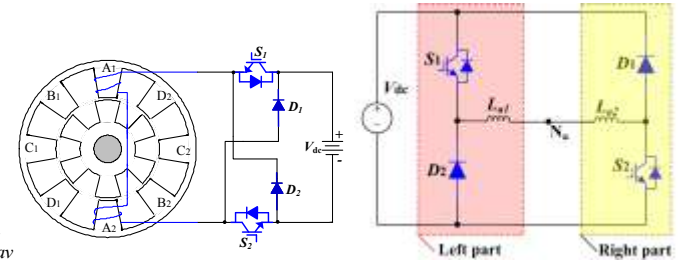
When part I or III is faulted, considering the proposed fault tolerance scheme in a CCC system, 3/4 part of the failure phase still can work to output torque. Although 1/4 part of the failure phase is out of work, the phase current is the control reference, it will be regulated to the same reference with the normal condition. In voltage-PWM control system, the phase voltage is employed as control reference, and the imposed voltage on each phase is the same. The current in the faulty phase will be larger than other healthy phases due to the decreased phase inductance. In order to reduce the unbalanced phase current further in voltage-PWM system, the turn-on angle of the failure phase can be used to adjust lagging to reduce the increased phase current in the failure winding, as illustrated in Fig. 13 (b). Therefore, the proposed fault tolerance technology can be employed to compensate the current and torque, and reduce the torque ripple to improve the drive performance in fault conditions.

IV. POPULARIZATION AND APPLICATION

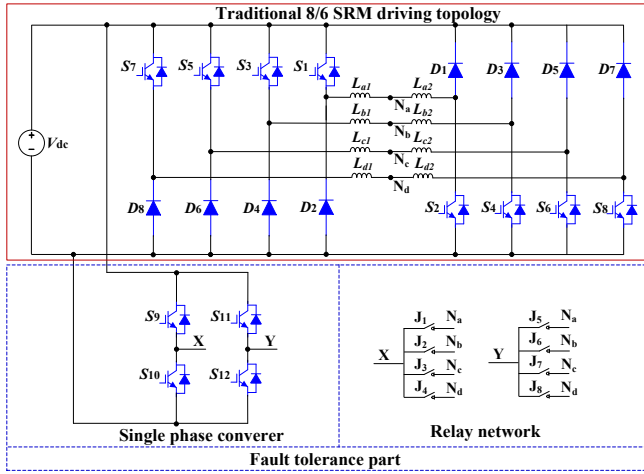
In addition to three-phase 12/8 SRM driving systems, four-phase 8-slot/6-pole (8/6) SRM driving systems are also widely used. The proposed fault tolerance also can be used in four phase 8/6 SRM.

A. Fault Tolerance Topology for Four Phase 8/6 SRM

Traditionally, for the 8/6 SRM, each phase is composed by two winding series connection, as shown in Fig. 14(a); for phase A, the connection node for two winding is marked as N_a , and the phase converter are divided by two parts, left part and right part, respectively, as presented in Fig. 14(b). The proposed fault tolerance topology is illustrated in Fig. 14(c), which is composed by signal phase converter and relay network.



(a) Phase converter of 8/6 SRM (b) Phase converter with winding central tapping node



(c) Proposed fault tolerance topology
Fig. 14. Fault tolerance topology for the 12/8 SRM.

B. Fault Tolerance Operation

Because the traditional 8/6 converter is composed by two parts, usually the fault can occur in either. The bridge arm composed by S_9 and S_{10} can block the left part fault; and the bridge arm composed by S_{11} and S_{12} can block the right part fault. The fault diagnosis process is similar to the 12/8 SRM driving system. Thanks to the relay network, when faulty part is located in faulty phase, the corresponding relay is switched on to block the faulty part. Fig. 15 is the typical hybrid faulty scenario in which each phase has fault; in traditional 8/6 SRM topology, the driving system can not work. By the proposed fault tolerance topology, the faulty 8/6 SRM still can operate with the new formed phase converter avoiding phase absence operation; and the states of phase windings in relation to the switching actions are illustrated in Table II.

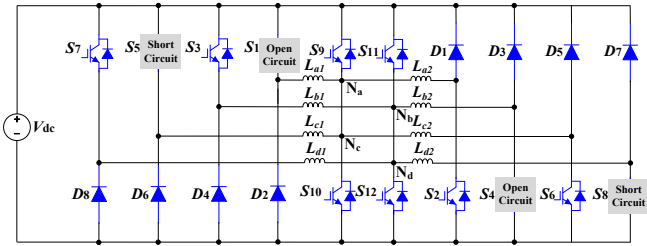


Fig. 15 Fault tolerance topology under hybrid fault scenario for the 8/6 SRM.

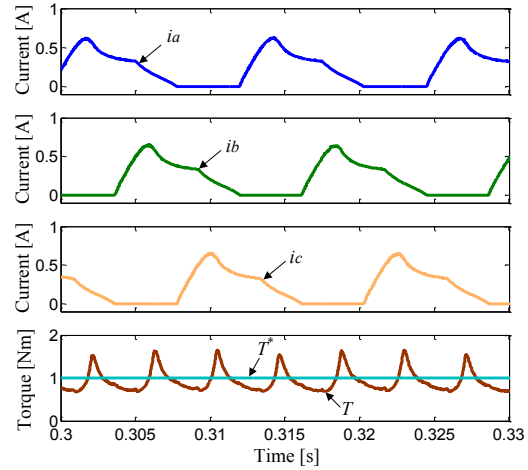
TABLE II RELATIONSHIP OF WORKING PHASE WITH SWITCHING DEVICES

Working phase	Conducting device	State of Phase
Phase A	S_9, S_2	Excitation
	S_{10}, D_1	Demagnetization
Phase B	S_3, S_{12}	Excitation
	D_4, S_{11}	Demagnetization
Phase C	S_9, S_6	Excitation
	S_{10}, D_5	Demagnetization
Phase D	S_7, S_{12}	Excitation
	D_8, S_{11}	Demagnetization

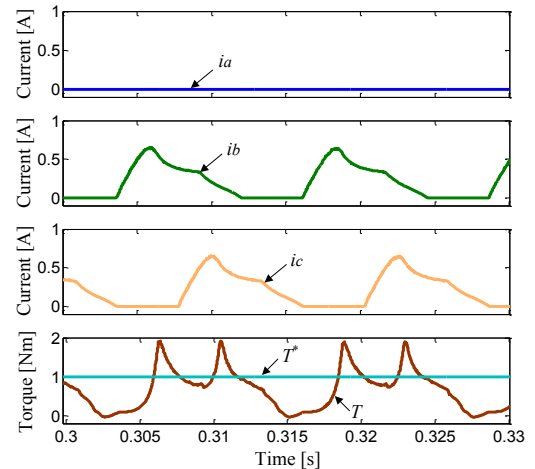
V. SIMULATION AND EXPERIMENT

In order to validate the proposed fault tolerance topology, a 750W 12/8 SRM is modeled in the Matlab/Simulation. Fig. 16 presents the simulation results of the 12/8 SRM in

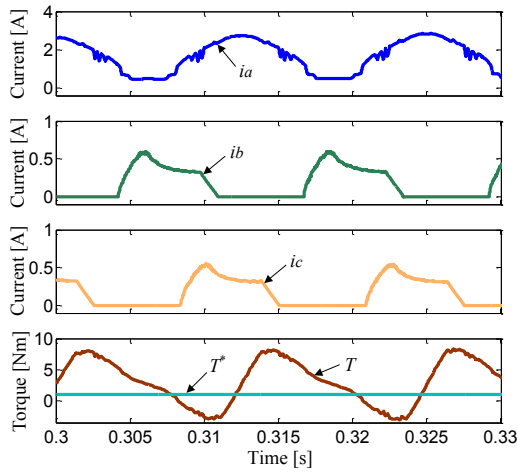
voltage-PWM control mode at 600 r/min under normal and faulty conditions. The turn-on and turn-off angles are set to 0° and 20° , respectively; the load torque is set to 1 N·m. In the waveforms, i_a , i_b , and i_c are the phase A, B, and C current, respectively. T and T^* are the instantaneous torque and given load torque, respectively. In the normal conditions, the three phase currents have the same shape with 15° phase-shift compare to each other, and the total torque is the sum of three phase torque, as shown in Fig. 16 (a). Fig.16 (b) shows the simulation results of switching devices open circuit fault condition of part I; thanks to the independence of each phase leg, the faulty phase will not affect the other healthy phase; while the torque ripple gets larger than that in normal conditions. Fig.16 (c) shows the simulation results of upper switching devices short circuit fault condition of phase A; the corresponding phase voltage cannot be regulated in phase turn-on region, and the demagnetization current also cannot flow to power supply in the phase turn-off region; therefore, phase A current is obviously larger than the normal phase, causing the torque ripple.



(a) Normal condition



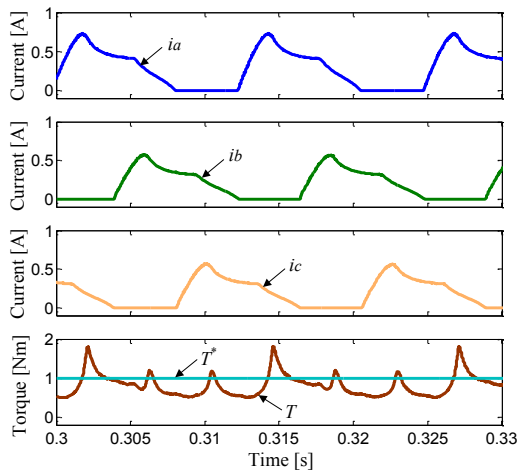
(b) Open fault of part I



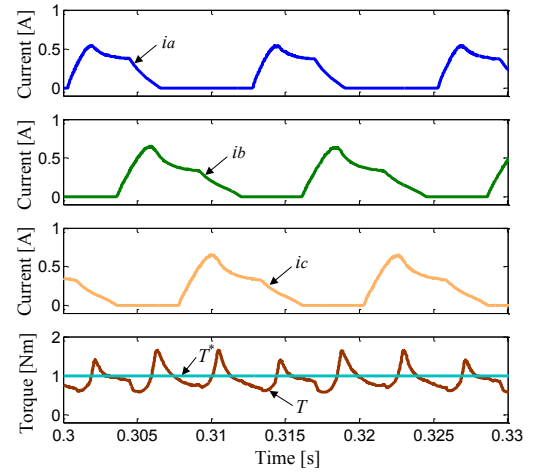
(c) Short fault of part I

Fig. 16. Simulation results of the 12/8 SRM in voltage-PWM control mode under normal and faulty conditions.

Fig. 17 illustrates the simulation results of the 12/8 SRM in voltage-PWM control mode at 600 r/min with fault tolerance topology under phase A faulty conditions. In Fig. 17(a), the current slope and peak value of phase A in the initial conduction region are $4/3$ of the normal value that coincides with theory analysis; although using the fault tolerant topology, the torque ripple is still large. In order to reduce torque ripple effectively, a fault tolerant scheme that lagging the turn-on angle of the fault phase is carried out, as presented in Fig. 17(b). The turn-on angle is set to 5° for phase A, and the torque ripple is clearly reduced compared to Fig. 17(a).



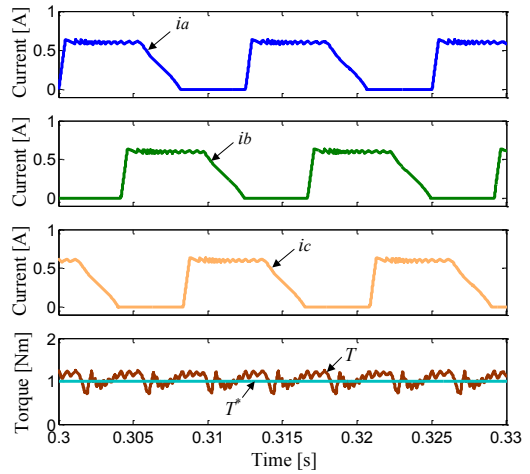
(a) Turn-on angle is 0° for phase A



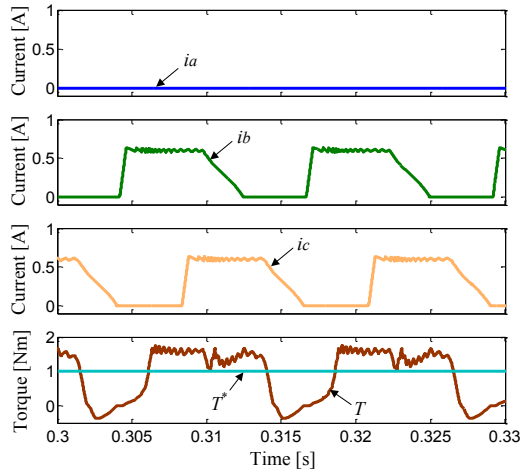
(b) Turn-on angle is 5° for phase A

Fig. 17. Simulation results of the 12/8 SRM in voltage-PWM control mode with fault tolerance topology under faulty conditions.

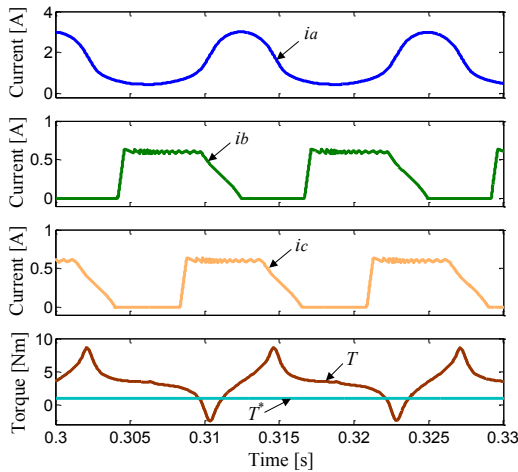
Fig. 18 illustrates the simulation results of the 12/8 SRM in CCC mode under normal and faulty conditions, respectively. In Fig. 18(a), the torque ripple is smaller than that of voltage-PWM control mode in normal condition shown in Fig. 16 (a). Fig. 18(b) and (c) are the simulation results under open and short-fault conditions that are similar to the voltage-PWM control mode. Fig. 19 presents the fault tolerance results in current regulation control mode at 600 r/min with the proposed fault tolerance topology. In current regulation control system, phase current is the control target, and it is regulated to the same reference compared to the normal one; and the torque ripple is effectively reduced to the normal condition compared to Fig. 18(a).



(a) Normal



(b) Open fault



(c) Short fault

Fig. 18. Simulation results of the 12/8 SRM in current regulation control mode with fault tolerance topology under faulty conditions.

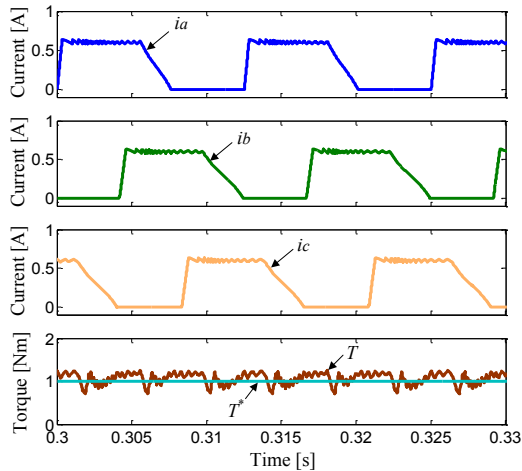


Fig. 19. Simulation results of the 12/8 SRM in CCC mode with fault tolerance topology under faulty conditions.

To verify the effectiveness of the proposed fault tolerance scheme, an experimental rig for testing a 12/8 and a 8/6 prototype SRM is set up, as shown in Fig. 20(a). The main motor parameters are illustrated Table III. Air switches are

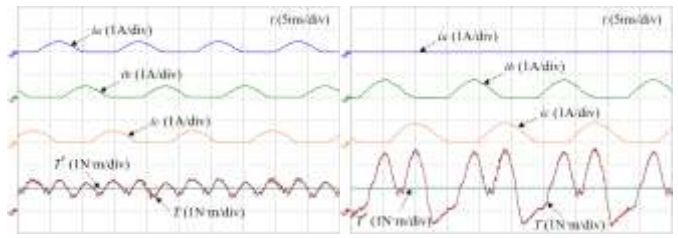
adopted to emulate open-circuit and short-circuit faults. The winding nodes are created and pulled out at the terminals when producing the prototype motor. An asymmetrical converter is employed in the system to drive the SRM, and a single phase converter is used to achieve the fault diagnosis and fault-tolerance operation. The switches are MOSFET FDA59N30; and diodes are IDW75E60. The hall current sensors (LA55Ps) are adopted to measure the phase currents. A 1000-line incremental encoder is used to measure the rotor position. A dSPACE 1006 platform is employed to implement the control algorithm. A magnetic brake acts as the load with a torque of 1 N·m. The dc-link voltage is fixed to 48 V. The torque observed in the oscilloscope is obtained online by using the real-time phase currents and rotor position to look up for the torque value in a 3-D torque table that includes the T - i - θ characteristics [33], [34]. The torque data in the lookup table is measured by using a rotor-clamping device when supplying different steady currents to the motor windings in a rotor position that changes step by step. The output torque in the experimental waveforms is observed through a D/A converter. Fig. 20(b) shows the fault tolerance control system diagram with the closed-loop speed regulation capability. As illustrated in the figure, a PI controller is employed to regulate the motor speed, and the proportional gain and integral gain are 0.05 and 0.5, respectively. The current controller and voltage controller are utilized to generate the drive signals to control the motor drive in different operation modes. The position detector and speed calculator are used to give the instantaneous speed for feedback control. The current sampling and fault diagnosis schemes are employed to control the gate signals for the fault tolerance topology to operate under faulted conditions.

TABLE III 12/8 AND 8/6 SRM SYSTEM PARAMETERS

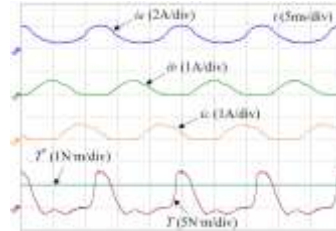
Parameters	Value for the 12/8 SRM	Value for the 8/6 SRM
Phase number	3	4
Number of stator poles	12	8
Number of rotor poles	8	6
Number of windings per phase	4	2
Rated speed (r/min)	1500	1500
Rated power (W)	750	150
Rated voltage (V)	200	132
Rated current (A)	3.6	1.1
Rated torque (N·m)	4.77	0.95
Phase resistance (Ω)	3.01	9.01
Minimum phase inductance (mH)	27.2	28.65
Maximum phase inductance (mH)	256.7	226.03
Rotor outer diameter (mm)	55	54
Rotor inner diameter (mm)	30	22
Stator outer diameter (mm)	102.5	102
Stator inner diameter (mm)	55.5	54.5
Core length (mm)	80	58
Stator arc angle (deg)	14	21
Rotor arc angle (deg)	16	24
Switching devices (MOSFET)	FDA59N30	
Diode	IDW75E60	

Figs. 21-24 present the experimental results of the 12/8 SRM at 600 r/min; and the turn-on and turn-off angles are set to 0° and 20° in the 12/8 SRM drive. In voltage-PWM control system with fault tolerance topology, the turn-on angle is set to 5° to improve the phase current balance for the fault tolerance

performance when the short-fault occurs. Fig.21 presents the typical voltage-PWM control model waveforms of the SRM under normal, open-circuit fault, and short-circuit fault conditions, respectively. Fig.21 (a) is the experimental waveform under normal condition; three phases have the same current amplitude and shape. Fig.21 (b) is the experimental result under open-circuit faulty condition without the proposed fault tolerance strategy; there is no current in the faulty phase; in a closed-loop system, when the open-fault happens, the other two phase currents are excited to be larger than the previous one by increasing the PWM duty-cycle, to compensate the absent phase torque. Fig.21 (c) presents the short-circuit faulty condition without the proposed fault tolerance strategy, in which the faulty phase current cannot decrease to zero; the experiment results have agreed well with the analytical study in Section II. Fig. 22 verifies the control strategy in voltage-PWM control mode under fault condition. As shown in Fig. 22 (a) and (b), by controlling the turn-on angle of the faulty phase, the output torque ripple can be decreased obviously. Fig. 23 presents the typical waveforms for the CCC model under normal, open fault, and short fault condition. In open-circuit faulty condition, there is no current in the faulty phase, as shown in Fig.23 (b); in short-circuit faulty condition, the fault phase current cannot decrease to zero, as shown in Fig.23 (c). With the proposed fault tolerance method, the faulty phase current and output torque can follow the reference values faithfully under CCC mode, as shown in Fig.24. Due to the symmetrical structure of part I and part III of phase converter (see Fig.1 (d)), part I fault has the same characteristics as part III fault.

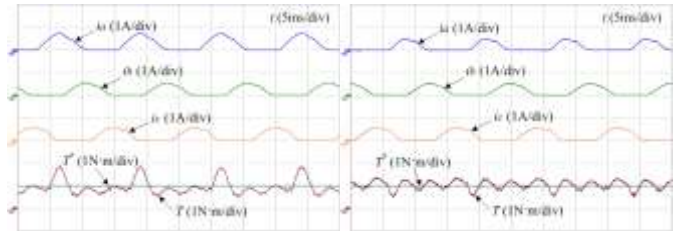


(a) Healthy condition (b) Open-circuit fault of part I without fault tolerance topology

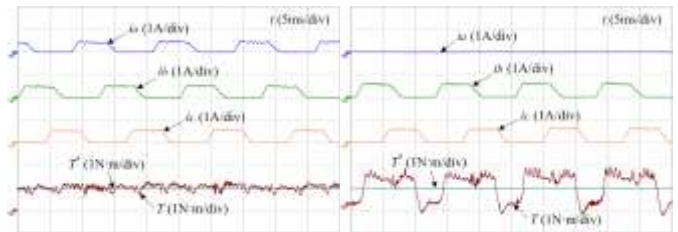


(c) Short-circuit fault of part I without fault tolerance topology

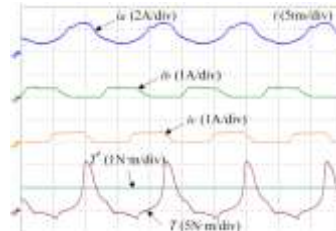
Fig. 21 Experimental results of the 12/8 SRM in voltage-PWM control mode under healthy and faulty conditions.



(a) 0° turn-on angle for phase A (b) 5° turn-on angle for phase A
Fig. 22. Experimental results of the 12/8 SRM in voltage-PWM control mode with fault tolerance topology under phase A fault conditions.

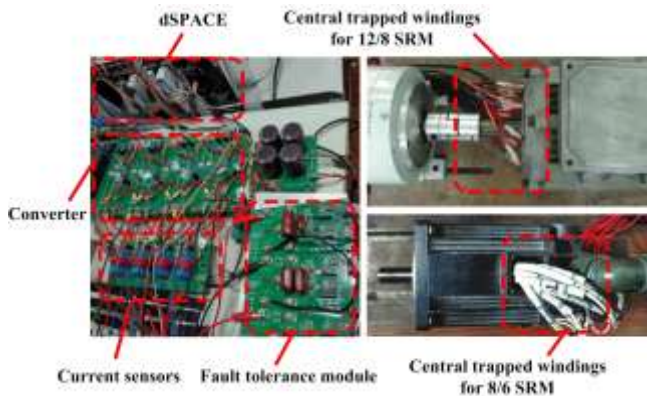


(a) Healthy (b) Open-circuit fault of part I without fault tolerance topology



(c) Short-circuit fault of part I without fault tolerance topology

Fig. 23. Experimental results of the 12/8 SRM in CCC mode without fault tolerance topology under phase A faulty conditions.



(a) Experimental setup.
(b) Diagram of the fault tolerance control system
Fig. 20. Experimental setup and the control system.

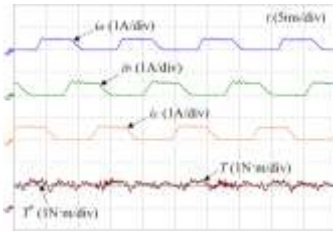


Fig. 24. Experimental results of the 12/8 SRM in CCC mode with fault tolerance topology under phase A faulty conditions.

Fig. 25 shows the fault tolerance operation at 600 r/min and 5 N·m load in CCC and voltage-PWM control modes under phase A part I fault condition. The system can still be stable when operating at large load and make up for the missing output torque of the fault phase. Fig. 26 shows the operation of the developed system during acceleration and at high speed with the 1 N·m load. As illustrated in Fig. 26(a), the speed follows the given value well during the continuous acceleration progress. In Fig. 26(b), the system is still stable when it is operated at 1500 r/min, which presents good stability.

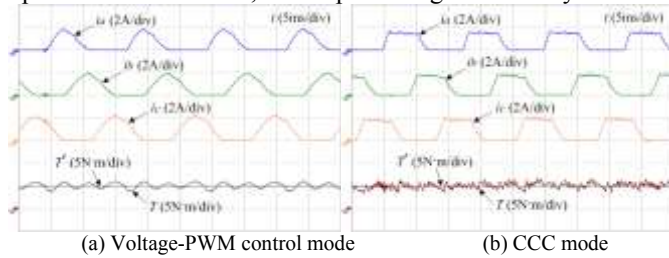


Fig. 25. Experimental results of the 12/8 SRM in fault tolerance operation under the high load.

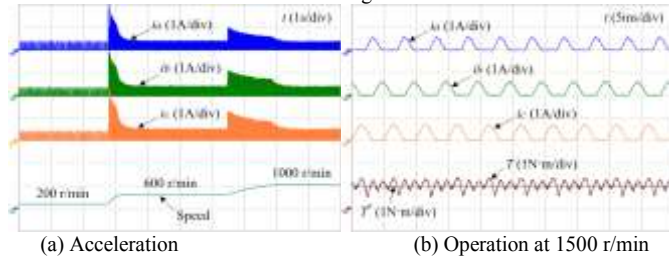
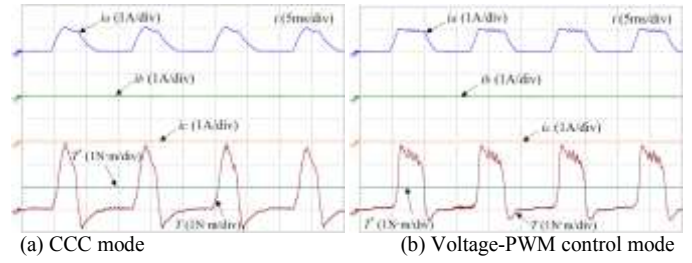
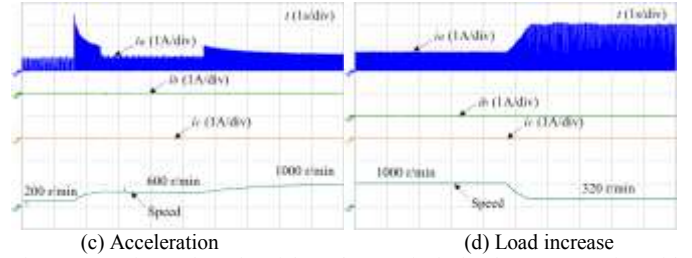


Fig. 26. Experimental results of the 12/8 SRM in fault tolerant operation during acceleration

Fig. 27 shows the fault tolerance operation with only a half phase winding at 600 r/min and 1 N·m load in CCC and voltage-PWM control modes, respectively. As shown in Fig. 27, only phase A has current, the other phases are out of work. The system can still operate with only a half phase winding at light load. Fig. 27 (c) and (d) illustrate the fault tolerance operation with only a half phase winding during acceleration and load increasing. The speed still follows the given speed well no matter during acceleration and in steady state, as shown in Fig. 27 (c). However, in Fig. 27(d), when the load increases from 1 to 3 N·m, the speed is reduced due to the insufficient load ability. Hence, in the extreme faulty conditions, the proposed fault tolerance scheme can still operate at light loads.

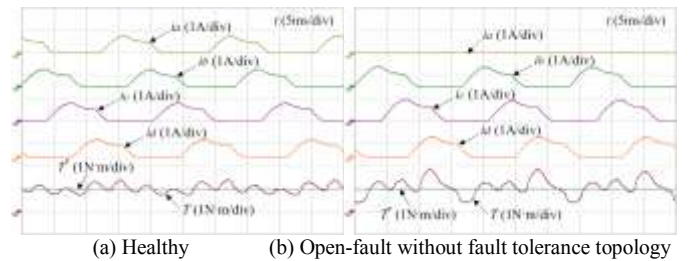


(a) CCC mode (b) Voltage-PWM control mode

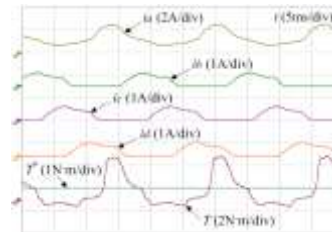


(c) Acceleration (d) Load increase
Fig. 27. Experimental results of the 12/8 SRM in fault tolerance operation with only a half phase winding in the extreme faulty condition at steady-state operation.

In order to verify the proposed fault tolerance scheme for the 8/6 SRM, the experimental tests are also carried out on a four-phase 8/6 SRM. Fig. 28 presents the operation waveforms under normal, open-circuit and short-circuit fault condition without the proposed fault tolerance strategy. The turn-on and turn-off angles are set to 0° and 28° . Fig. 29 shows the experimental waveforms with the proposed fault tolerance strategy. In voltage-PWM control system with fault tolerance topology, the turn-on angle is set to 8° to improve the phase current balance for the fault tolerance performance when the short-fault occurs, as shown in Fig.29 (b). By the proposed fault tolerance strategy, the torque ripple is limited in low ripple and the fault phase still can work as normal phases; therefore, the proposed fault tolerance strategy still can apply in 8/6 SRM. The only difference is that a phase winding can be divided into two parts for 8/6 motor, while it is divided into three parts for the 12/8 SRM.



(a) Healthy (b) Open-fault without fault tolerance topology



(c) Short-fault without fault tolerance topology

Fig. 28 Experimental results of the 8/6 SRM in voltage-PWM control mode without fault tolerance topology under normal and faulty conditions.

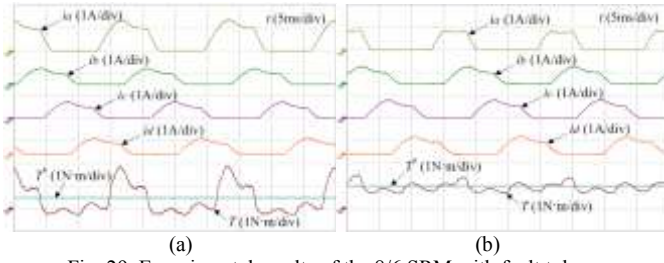


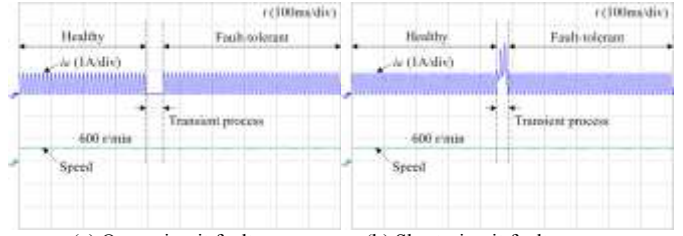
Fig. 29. Experimental results of the 8/6 SRM with fault tolerance topology under faulty conditions. (a) Fault tolerance operation under voltage PWM control mode. (b) Turn-on angle is 8° for phase A

Table IV presents a comparison of torque ripples with and without the proposed fault tolerance strategy. It can be seen that the proposed fault tolerance strategy is effective in reducing the torque ripples. For example, under a single-switch open-circuit fault and CCC control mode, the torque ripple is $3.1 \text{ N}\cdot\text{m}$ without fault tolerance strategy, which is nearly 6 times higher than its healthy condition. The torque ripple is reduced to $0.56 \text{ N}\cdot\text{m}$ when the proposed fault tolerance strategy is implemented. When a single-switch short circuit occurs, the torque ripple is $8.2 \text{ N}\cdot\text{m}$ without fault tolerance strategy, which is over 15 times of its healthy condition. It is reduced to only $0.56 \text{ N}\cdot\text{m}$ with the proposed fault tolerance strategy.

TABLE IV COMPARISON OF TORQUE RIPPLE WITH AND WITHOUT FAULT TOLERANCE STRATEGY

Parameter	Without fault tolerance (CCC)	With fault tolerance (CCC)	Without fault tolerance (PWM)	With fault tolerance (PWM)
Healthy condition	$0.53 \text{ N}\cdot\text{m}$	$0.53 \text{ N}\cdot\text{m}$	$0.41 \text{ N}\cdot\text{m}$	$0.41 \text{ N}\cdot\text{m}$
Single-switch open circuit	$3.1 \text{ N}\cdot\text{m}$	$0.56 \text{ N}\cdot\text{m}$	$1.96 \text{ N}\cdot\text{m}$	$0.46 \text{ N}\cdot\text{m}$
Single-switch short circuit	$8.2 \text{ N}\cdot\text{m}$	$0.56 \text{ N}\cdot\text{m}$	$7.5 \text{ N}\cdot\text{m}$	$0.46 \text{ N}\cdot\text{m}$
All-switch faulted condition	No torque generated	$3.88 \text{ N}\cdot\text{m}$	No torque generated	$3.46 \text{ N}\cdot\text{m}$

Fig. 30 presents a transient progress of the system with the proposed fault tolerance strategy. Fig. 30(a) and (b) illustrate the progress of open-circuit fault and short-circuit fault, respectively. Within 50 ms upon a fault, the proposed strategy can realize fault detection and the system can operate with the fault. Fig. 31 shows the efficiency of the SRM drive under healthy condition, with fault tolerance condition and without fault tolerance condition. For this low-power SRM prototype, the system efficiency is relatively low [38]-[41]. However, it is still very clear that the proposed fault tolerance strategy can improve the system efficiency under faulty conditions. The proposed method can effectively bypass the faulted component while still operating with healthy components in the faulted phase. Without such a fault tolerance strategy, the faulted phase is lost and the system efficiency is very low.



(a) Open-circuit fault (b) Short-circuit fault
Fig. 30 Fault diagnosis and fault tolerance progress.

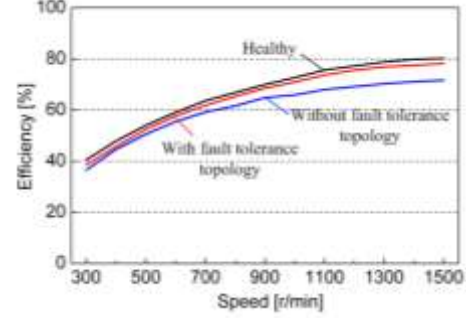


Fig. 31 SRM efficiency.

VI. CONCLUSION

In this paper, a novel flexible topology is introduced to improve the reliability of SRM drive systems for EV/HEV applications. The main contributions of this paper are: (i) fault tolerance is achieved by developing a modular and low cost structure, without changing traditional SRM driving topology; (ii) by the introduction of winding nodes, the traditional asymmetrical half bridge topology is divided into three parts; by switching on fault tolerance part, fault diagnosis can be achieved easily; (iii) for part I or part III fault, the proposed fault tolerance topology only reduce 1/4 output. (iv) when a fault occurs in one phase or faults occur in all phases, the SRM drive can still operate with the healthy parts of the faulted phases; and the improved fault tolerance operation control strategy is proposed to decrease the influence of the faulty; (v) the proposed fault tolerance solution can be used in 12/8 and 8/6 SRMs, and only needs two fault tolerance half bridges. The developed technology can improve the reliability and cost-efficiency of the SRM drive for EV/HEVs, as well as electric aircraft and ships.

REFERENCES

- [1] B. K. Bose, "Global energy scenario and impact of power electronics in 21st century," *IEEE Trans. Ind. Electron.*, vol. 60, no. 7, pp. 2638-2651, Jul. 2013.
- [2] S. Yantao, and W. Bingsen, "Evaluation methodology and control strategies for improving reliability of HEV power electronic system," *IEEE Trans. Veh. Technol.*, vol. 63, no. 8, pp. 3661-3676, Oct. 2014.
- [3] P. Pisek, B. Stumberger, T. Marcic, and P. Virtic, "Design analysis and experimental validation of a double rotor synchronous PM machine used for HEV," *IEEE Trans. Magn.*, vol. 49, no. 1, pp. 152-155, 2013.
- [4] K. Kiyota, T. Kakishima, A. Chiba, "Comparison of test result and design stage prediction of switched reluctance motor competitive with 60-kW rare-earth PM motor," *IEEE Trans. Ind. Electron.*, vol. 61, no. 10, pp. 5712 - 5721, Oct. 2014.
- [5] H. Jinsook, L. Heekwang, and N. Kwanghee, "Charging method for the secondary battery in dual-inverter drive Systems for electric vehicles," *IEEE Trans. Power Electron.*, vol. 30, no. 2, pp. 909-921, Feb. 2015.

- [6] Y. Hu, X. Song, W. Cao, and B. Ji, "New SR drive with integrated charging capacity for plug-in hybrid electric vehicles (PHEVs)," *IEEE Trans. Ind. Electron.*, vol. 61, no. 10, pp. 5722-5731, Oct. 2014.
- [7] I. Boldea, L. N. Tutelea, L. Parsa, and D. Dorrell, "Automotive electric propulsion systems with reduced or no permanent magnets: an overview," *IEEE Trans. Ind. Electron.*, vol. 61, no. 10, pp. 5696-5711, Oct. 2014.
- [8] D. H. Lee, T. H. Pham, J. W. Ahn, "Design and operation characteristics of four-two pole high-speed SRM for torque ripple reduction," *IEEE Trans. Ind. Electron.*, vol. 60, no. 9, pp. 3637-3643, Sep. 2013.
- [9] L. Shen, J. Wu, and S. Yang, "Initial position estimation in SRM using bootstrap circuit without predefined inductance parameters," *IEEE Trans. Power Electron.*, vol. 26, no. 9, pp. 2449-2456, Sep. 2011.
- [10] J. Liang, D. H. Lee, G. Xu, J. W. Ahn, "Analysis of passive boost power converter for three-phase SR drive," *IEEE Trans. Ind. Electron.*, vol. 57, no. 9, pp. 2961-2971, Sep. 2010.
- [11] M. Takeno, A. Chiba, N. Hoshi, S. Ogasawara, M. Takemoto, and M. A. Rahman, "Test results and torque improvement of the 50-kW switched reluctance motor designed for hybrid electric vehicles," *IEEE Trans. Ind. Appl.*, vol. 48, no. 4, pp. 1327-1334, Jul./Aug. 2012.
- [12] C. Gan, J. Wu, S. Yang, Y. Hu, "Phase current reconstruction of switched reluctance motors from dc-link current under double high frequency pulses injection" *IEEE Trans. Ind. Electron.*, vol. 62, no. 5, pp. 3265 – 3276, May 2015.
- [13] B. Ji, W. Cao, P. Volker, X. Song, Y. Hu, P. Gareth, "In-situ diagnostics and prognostics of solder fatigue in IGBT modules for electric vehicle drives," *IEEE Trans. Power Electron.*, vol. 30, no. 3, pp. 1535–1543, Mar. 2015.
- [14] B. Ji, W. Cao, X. Song, Y. Hu, V. Pickert, "Multi-objective design of IGBT power modules considering power cycling and thermal cycling," *IEEE Trans. Power Electron.*, vol. 30, no. 5, pp. 2493-2504, May 2015.
- [15] H. Torkaman, E. Afjei, and P. Yadegari, "Static, dynamic, and mixed eccentricity faults diagnosis in switched reluctance motors using transient finite element method and experiments," *IEEE Trans. Magn.*, vol. 48, no. 8, pp. 2254-2264, Aug. 2012.
- [16] N. S. Gameiro, and A. J. Marques Cardoso, "A new method for power converter fault diagnosis in SRM drives," *IEEE Trans. Ind. Appl.*, vol. 48, no. 2, pp. 653-662, Mar/Apr. 2012.
- [17] C. Hao, and L. Shengli, "Fault diagnosis digital method for power transistors in power converters of switched reluctance motors," *IEEE Trans. Ind. Electron.*, vol. 60, no. 2, pp. 749-763, Feb. 2013.
- [18] J. F. Marques, J. O. Estima, N. S. Gameiro, and A. M. Cardoso, "A new diagnostic technique for real-time diagnosis of power converter faults in switched reluctance motor drives," *IEEE Trans. Ind. Appl.*, vol. 50, no. 3, pp. 1854-1860, May/June. 2014.
- [19] N. S. Gameiro, and A. J. M. Cardoso, "Fault tolerant control strategy of SRM drives," *IEEE International Symposium on Power Electronics, Electrical Drives, Automation and Motion*, Ischia, Italy, pp. 301-306, Jun. 2008.
- [20] A. A. Arkadan, P. Du, M. Sidani, and M. Bouji, "Performance prediction of SRM drive systems under normal and fault operating conditions using GA-based ANN method," *IEEE Trans. Magn.*, vol. 36, no. 4, pp. 1945-1949, July. 2000.
- [21] M. Bouji, A. A. Arkadan, and T. Ericsen, "Fuzzy inference system for the characterization of SRM drives under normal and fault conditions," *IEEE Trans. Magn.*, vol. 37, pp. 3745-3748, Sep. 2001.
- [22] A. A. Arkadan, and B. W. Kielgas, "Switched reluctance motor drive systems dynamic performance prediction under internal and external fault conditions," *IEEE Trans. Energy Convers.*, vol. 9, no. 1, pp. 45-52, Mar. 1994.
- [23] B. Lequesne, S. Gopalakrishnan, and A. M. Omekanda, "Winding short circuits in the switched reluctance drive," *IEEE Trans. Ind. Appl.*, vol. 41, no. 5, pp. 1178-1184, Sep/Oct. 2005.
- [24] H. Torkaman, and E. Afjei, "Comprehensive detection of eccentricity fault in switched reluctance machines using high-frequency pulse injection," *IEEE Trans. Power Electron.*, vol. 28, no. 3, pp. 1382-1390, Mar. 2013.
- [25] M. D. Hennen, M. Niessen, C. Heyers, H. J. Brauer, and R. W. De Doncker, "Development and control of an integrated and distributed inverter for a fault tolerant five-phase switched reluctance traction drive," *IEEE Trans. Power Electron.*, vol. 27, no. 2, pp. 547-554, Feb. 2012.
- [26] A. Labak, and N. C. Kar, "Designing and prototyping a novel five-phase pancake-shaped axial-flux SRM for electric vehicle application through dynamic FEA incorporating flux-tube modeling," *IEEE Trans. Ind. Appl.*, vol. 49, no. 3, pp. 1276-1288, May/June. 2013.
- [27] W. Ding, Y. Liu, Y. Hu, "Performance evaluation of a fault-tolerant decoupled dual-channel switched reluctance motor drive under open-circuits," *IET Electric Power Applications*, vol. 8, no. 4, pp. 117-130, Apr. 2014.
- [28] M. Ruba, I. A. Viorel, Szabo, x, and L., "Modular stator switched reluctance motor for fault tolerant drive systems," *IET Electric Power Applications*, vol. 7, no. 3, pp. 159-169, Mar. 2013.
- [29] L. Szabo, and M. Ruba, "Segmental stator switched reluctance machine for safety-critical applications," *IEEE Trans. Ind. Appl.*, vol. 48, no. 6, pp. 2223-2229, Nov/Dec. 2012.
- [30] H. Torkaman, E. Afjei, and M. S. Toulabi, "New double-layer-per-phase isolated switched reluctance motor: concept, numerical analysis, and experimental confirmation," *IEEE Trans. Ind. Electron.*, vol. 59, no. 2, pp. 830-838, Feb. 2012.
- [31] N. S. Gameiro, A. J. M. Cardoso, "Fault Tolerant Power Converter for Switched Reluctance Drives," *18th International Conference on Electrical Machines*, Algarve, Portugal, pp. 1-6, Sept. 2008.
- [32] M. Ruba, C. Oprea, L. Szabó, "Comparative study on switched reluctance machine based fault-tolerant electrical drive systems," *IEEE International Conference on Electric Machines and Drives 2009*, Miami, USA, pp. 987-992, May 2009.
- [33] A. C. Oliveira, C. B. Jacobina, A. M. N. Lima, and F. Salvadori, "Startup and fault tolerance of the SRM drive with three-phase bridge inverter," *IEEE Conference in Power Electronics Specialists*, 2005, Recife, Brazil, pp. 714-719, Jun. 2005.
- [34] L. A. Belfore, II, and A. Arkadan, "A methodology for characterizing fault tolerant switched reluctance motors using neurogenetically derived models," *IEEE Trans. Energy Convers.*, vol. 17, no. 3, pp. 380-384, Sep. 2002.
- [35] S. Mir, M. S. Islam, T. Sebastian, and I. Husain, "Fault-tolerant switched reluctance motor drive using adaptive fuzzy logic controller," *IEEE Trans. Power Electron.*, vol. 19, no. 2, pp. 289-295, Mar. 2004.
- [36] W. Wang, B. Fahimi, "Fault resilient strategies for position sensorless methods of switched reluctance motors under single and multiphase fault," *IEEE Journal of Emerging and Selected Topics in Power Electronics*, vol. 2, no. 2, pp. 190-200, Jun. 2014.
- [37] Hu, Y., Gan, C., Cao, W., Li, W., and Finney, S., "Central-tapped node linked modular fault tolerance topology for SRM applications," *IEEE Trans. Power Electron.*, vol. PP, no. 99, pp. 1,1, in press.
- [38] K. M. Rahman, and S. E. Schulz, "Design of high-efficiency and high-torque-density switched reluctance motor for vehicle propulsion," *IEEE Trans. Ind. Appl.*, vol. 38, no. 6, pp. 1500-1507, Nov./Dec. 2002.
- [39] D. H. Lee, J. Liang, Z. G. Lee, and J. W. Ahn, "A Simple nonlinear logical torque sharing function for low-torque ripple SR drive," *IEEE Trans. Ind. Electron.*, vol. 56, no. 8, pp. 3021-3028, Aug. 2009.
- [40] J. Liang, D. H. Lee, G. Xu, and J. W. Ahn, "Analysis of passive boost power converter for three-phase SR drive," *IEEE Trans. Ind. Electron.*, vol. 57, no. 9, pp. 2961-2971, Sep. 2010.
- [41] H. Y. Yang, Y. C. Lim, and H. C. Kim, "Acoustic noise/vibration reduction of a single-phase SRM using skewed stator and rotor," *IEEE Trans. Ind. Electron.*, vol. 60, no. 10, pp. 4292-4300, Oct. 2013.



Yihua Hu (M'13-SM'15) received the B.S. degree in electrical motor drives in 2003, and the Ph.D. degree in power electronics and drives in 2011, both from China University of Mining and Technology, Jiangsu, China. Between 2011 and 2013, he was with the College of Electrical Engineering, Zhejiang University as a Postdoctoral Fellow. Between November 2012 and February 2013, he was an academic visiting scholar with the School of Electrical and Electronic Engineering, Newcastle University, Newcastle upon Tyne, UK. He is currently a research associate with the Department of Electronic & Electrical Engineering, University of Strathclyde, Glasgow, UK. He has published more than 50 technical papers in leading journals and conference proceedings. His research interests include PV generation system, power electronics converters & control, and electrical motor drives.



Chun Gan (S'14) received B.S. and M.S. degrees in power electronics and drives from China University of Mining and Technology, Jiangsu, China, in 2009 and 2012, respectively. He is currently working toward Ph.D. degree in the College of Electrical Engineering, Zhejiang University, Hangzhou, China.

His research interests include electrical motor drives, motor design, control with emphasis on switched reluctance motor sensorless technique, and optimization of the torque ripple and efficiency of the motor system.

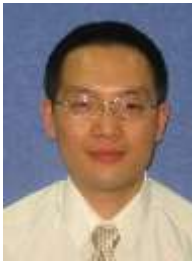


Stephen J. Finney received the M.Eng. degree from Loughborough University of Technology, Loughborough, U.K., in 1988 and the Ph.D. degree from Heriot-Watt University, Edinburgh, U.K., in 1995. For two years, he was with the Electricity Council Research Centre laboratories near Chester, U.K. He is currently a Professor with the University of Strathclyde, Glasgow, U.K. His areas of research interest are HVDC, MMC, renewable generation, and electrical vehicle.



Wenping Cao (M'05-SM'11) received the B.Eng. in electrical engineering from Beijing Jiaotong University, Beijing, China, in 1991; and the Ph.D. degree in electrical machines and drives from the University of Nottingham, Nottingham, U.K., in 2004. He is currently a Senior Lecturer with Queen's University Belfast, Belfast, U.K. His research interests include thermal performance and fault analysis of electric machines, drives and power electronics.

Dr. Cao is the recipient of the Best Paper Award at the LDIA'13 Conference. He serves as an Associate Editor for IEEE TRANSACTIONS ON INDUSTRY APPLICATIONS, *IEEE Industry Applications Magazine*, *IET Power Electronics*, and nine other International Journals. He is also a member of the Institution of Engineering and Technology and a Fellow of Higher Education Academy.



Jiangfeng Zhang obtained his BSc and PhD in computing mathematics and applied software from Xi'an Jiaotong University, China, in July 1995 and December 1999, respectively. He is a senior lecturer at the Department of Electronic and Electrical Engineering, University of Strathclyde. He is also a member of the IFAC TC6.3 (Power and Energy Systems). His research interests include optimization modelling and control of energy systems, with a focus

on energy efficiency and demand side management.



Wuhua Li (M'09) received the B.Sc. and Ph.D. degree in Applied Power Electronics and Electrical Engineering from Zhejiang University, Hangzhou, China, in 2002 and 2008, respectively. From September 2004 to March 2005, he was a Research Intern, and from January 2007 to June 2008, a Research Assistant in GE Global Research Center, Shanghai, China. From July 2008 to April 2010, he joined the College of Electrical Engineering, Zhejiang University as a Post doctor. In May 2010, he became a faculty member at Zhejiang University

as a Lecturer. In December 2010, he was promoted as an Associate Professor. From July 2010 to September 2011, he was a Ryerson University Postdoctoral Fellow with the Department of Electrical and Computer Engineering, Ryerson University, Toronto, ON, Canada. His research interests include high efficiency power converters and renewable energy power conversion system. Dr. Li has published more than 100 peer-reviewed technical papers and holds over 20 issued/pending patents.

Due to his excellent teaching and research contributions, Dr. Li received the 2011 TOP TEN Excellent Young Staff Award and the 2012 Distinguished Young Scholar from Zhejiang University, the 2012 Outstanding Young Researcher Award from Zhejiang Province, the 2012 Delta Young Scholar from Delta Environmental & Educational Foundation and the 2012 National Outstanding Young Scholar. He received three Scientific and Technological Achievements Awards from Zhejiang Provincial Government and the State Educational Ministry of China in 2009 and 2011, respectively.